Robotic Neuro-Endoscope with Concentric Tube Augmentation

Evan J. Butler [Member, IEEE],
Sterling Point Research LLC, Winchester MA 01890 USA

Robert Hammond-Oakley,
Sterling Point Research LLC, Winchester MA 01890 USA

Szymon Chawarski,
Sterling Point Research LLC, Winchester MA 01890 USA

Andrew H. Gosline [Member, IEEE],
Cardiovascular Surgery, Children's Hospital Boston, Harvard Medical School, Boston MA 02115 USA

Patrick Codd,
Neurosurgery, Children's Hospital Boston, Harvard Medical School, Boston MA 02115 USA

Tomer Anor,
Neurosurgery, Children's Hospital Boston, Harvard Medical School, Boston MA 02115 USA

Joseph R. Madsen,
Neurosurgery, Children's Hospital Boston, Harvard Medical School, Boston MA 02115 USA

Pierre E. Dupont, Fellow, IEEE, and
Cardiovascular Surgery, Children's Hospital Boston, Harvard Medical School, Boston MA 02115 USA

Jesse Lock, Member, IEEE
Sterling Point Research LLC, Winchester MA 01890 USA

Evan J. Butler: evan.butler@sterlingpointresearch.com; Robert Hammond-Oakley: robert.hammond@sterlingpointresearch.com; Szymon Chawarski: szymon.chawarski@sterlingpointresearch.com; Andrew H. Gosline: andrew.gosline@childrens.harvard.edu; Patrick Codd: patrick.codd@childrens.harvard.edu; Tomer Anor: tomer.anor@childrens.harvard.edu; Joseph R. Madsen: joseph.madsen@childrens.harvard.edu; Pierre E. Dupont: pierre.dupont@childrens.harvard.edu; Jesse Lock: jesse.lock@sterlingpointresearch.com

Abstract

Surgical robots are gaining favor in part due to their capacity to reach remote locations within the body. Continuum robots are especially well suited for accessing deep spaces such as cerebral ventricles within the brain. Due to the entry point constraints and complicated structure, current techniques do not allow surgeons to access the full volume of the ventricles. The ability to access the ventricles with a dexterous robot would have significant clinical implications. This paper presents a concentric tube manipulator mated to a robotically controlled flexible endoscope. The device adds three degrees of freedom to the standard neuroendoscope and roboticizes the entire package allowing the operator to conveniently manipulate the device. To demonstrate the improved functionality, we use an in-silica virtual model as well as an ex-vivo anatomic model of a patient with a treatable form of hydrocephalus. In these experiments we demonstrate that the augmented and roboticized endoscope can efficiently reach critical regions that a manual scope cannot.

I. Introduction

Surgical robots have become a mainstream tool for many physicians in the past decade. Laparoscopic robotic systems from companies like *Intuitive Surgical Systems, DLR* and others have demonstrated that robotic technology can measurably improve certain surgical procedures [1]. One of the principal benefits of these robots is that they can operate with precision and efficiency in tight spaces (such as an enclosed abdomen) where a surgeon's hands cannot. This attribute becomes particularly valuable during minimally invasive surgery (MIS), where the goal is to access and manipulate deep internal structures while limiting collateral tissue damage.

Several types of novel robots have been specifically developed to address the constraints of MIS. Given the difficulty of access and the narrow passageways through which these procedures are performed, it is often appropriate to use robotic designs that eschew traditional long and rigid linkages in favor of flexible curving segments. These 'continuum' or 'snake-like' robotic designs include concentric tube robots and tendon driven robots. A concentric tube robot is comprised of several pre-curved concentric tubes of varying flexibility [2]. By controlling the translation and rotation of each tube at the base of the robot, the tip of the robot as well as its overall shape can be controlled. Precise control relies on advanced kinematic models to account for a variety of phenomena, including bending, torsion, nonlinear constitutive effects, friction, material hysteresis, and clearance [3] [4] [5]. One style of 'joint' mechanism is shown in Fig. 1.

In contrast, the components of similarly sized snake-like tendinous robots generally consist of multiple small discrete mechanical components that may be controlled at a distance through a long and arbitrarily flexing region [6] [7].

Medical endoscopes fall into this latter category of devices. Modern endoscopes are composed of a long (~40–250 cm) and narrow (3–15 mm OD) flexible sheath, housing combinations of lumens, optical components, and other sensors. The distal end may have one or two mechanized degrees of freedom generating a two or three dimensional curvature. These controls are driven by a tendinous system as shown in Fig. 2. Tools may be inserted through the lumen and controlled from the proximal end of the scope.

Neurosurgical procedures require a high level of precision and dexterity, as structures in the brain are especially delicate and valuable to the long-term health of the patient. Most previous neurosurgical robotic applications have conformed to a standard surgical approach. As an example, the NeuroArm system is a two-handed teleoperated neurosurgical robot that utilizes the same tools and techniques of manual open surgery [19]. Thus, the robotic procedure still relies on an open craniotomy and wide exposure to allow the robot access to the brain. As a second example, the NeuRobot is a robotic endoscope consisting of a straight 10 mm diameter shaft containing three instrument ports that can be used to deploy a laser and up to two 3 DOF forceps [20]. This device is limited to the subset of procedures that can be performed with a straight rigid endoscope. Two recent efforts have attempted to achieve greater steerability through robotics [21] [22]. These devices consist of several segments connected by current-controlled SMA actuators that contain working channels for tool delivery. While capturing the need for flexibility, these designs are comparatively bulky relative to current endoscopic standards.

Accessing the most central structures of the brain with minimal tissue disturbance is particularly difficult. While narrow neuroendoscopes have been developed to pass through the cortex and into the cerebral ventricles, their inherent flexible design limits the workspace and controllability. Significant portions of the ventricular anatomy are unreachable, despite the limited volume of the space. These endoscopes are difficult to manipulate and require

two hands at all times. The addition of multiple degrees of freedom to the manual endoscope exceeds the limits of human control.

The contribution of this paper is to demonstrate that concentric tube robot technology can be used to great effect in combination with other steerable continuum mechanisms, such as endoscopes and catheters, to increase the effective workspace of the system. Furthermore, it is shown that robotic control of a manual neuroendoscope not only provides safer and smoother control of the original scope degrees of freedom; it also provides the means to integrate the control of the concentric tube degrees of freedom. These capabilities are illustrated in the context of a specific neuroendoscopic procedure: endoscopic third ventriculostomy and choroid plexus cauterization. Computer-based 3D models are used to design the concentric tubes to achieve the desired procedural workspace and the robot design is verified through navigation experiments in an anatomically accurate phantom model of the ventricles.

II. Procedure Background

A. Neurological Applications for Endoscopes

Recent advances in optical technology have led to the rapidly increasing use of endoscopes in neurosurgical procedures involving the central ventricles. Specific pathologies that may be accessed through the ventricles include hydrocephalus [8][9][10][11][12], infectious and cystic lesions [13] [14], intraventricular hematomas [13], and other tumors [15][16][17]. While some intraventricular procedures are performed using current technology, most definitive surgical treatment requires more invasive technique. Dexterous minimally-invasive navigation within the ventricles and the surrounding tissue remains an unmet challenge.

Hydrocephalus is a condition that may be treated using a flexible endoscope. This condition is characterized by abnormal homeostasis of cerebrospinal fluid (CSF), a clear, watery substance that is produced within the ventricles by the choroid plexus. CSF fills the ventricles and surrounds the brain and spinal cord, acting as a support and cushion for the neural structures. Patients with hydrocephalus accumulate excess CSF, which eventually leads to a displacement of neural tissue. Over 69,000 people are diagnosed with hydrocephalus each year [18]. Left untreated, hydrocephalus can lead to progressive elevation in intracranial pressure, neurologic injury, and even death.

An endoscopic procedure pioneered by Warf for the treatment of hydrocephalus has provided a promising method for the treatment of some forms of this disease. The procedure, endoscopic third ventriculostomy (ETV) and choroid plexus cauterization (CPC), proceeds as follows. First, the ventricles are accessed using a rigid cannula introduced through a small burr hole in the skull. Next, a flexible endoscope is introduced and used to create a hole in the floor of the third ventricle, giving the CSF an additional route of egress from the ventricular space. Lastly, a wire low-voltage monopolar cautery device is manually deployed through the endoscope and used to ablate the choroid plexus. The goal of the procedure is to remove sufficient choroid so as to significantly reduce CSF production. It is the current clinical practice to ablate as much of the choroid as possible.

While ETV in isolation can be performed without the use of flexible endoscopy or complex intraventricular navigation, it has been shown that ETV is less effective in isolation in children under 1 year of age [8]. It was also shown that the combined ETV/CPC procedure is more effective in treating hydrocephalus without a shunt in this patient group, including 76% success rate with ETV/CPC when compared with 35% success with ETV alone [10] [11][12].

This technique is not without significant drawbacks. Currently available flexible endoscopes lack the ability to completely navigate the complex, small ventricular geometry and hence ablate the entire choroid plexus. Navigation of the flexible endoscope itself requires complex coordination of scope rotations, translations, tip movements, and tool actuations that are ergonomically difficult to achieve during the course of the procedure. Precise manipulations are essential to successfully navigate the ventricles without damaging the delicate surrounding brain tissue. These complex manually driven manipulations poses a significant challenge for the surgeon, creating a potentially prohibitive learning curve that would preclude the ability to employ this important procedure in an accurate and safe manner. Expanding this access, and providing instrumentation capable of easing the learning curve could broaden the application of the ETV/CPC procedure and potentially expand treatment options for a multitude of patients.

III. Robot Design

A. Robot Overview and Properties

A robotic endoscope was designed to address the above clinical need. The robot is comprised of two main components: an exoskeleton designed to contain and manipulate a manual endoscope (Karl Storz Steerable Neuro-Fiberscope Model # 11282 BN) shown in Fig. 4, and a tool manipulator. This approach ensures that the surgeon is familiar with the basic operation of the endoscope, while maintaining access to the built-in optics system and tool channels.

The robotic endoscope can be characterized as a series of distinct segments as shown in Fig. 5. Section A is the initial portion of the scope neck; it is flexible, but torsionally rigid. Section B is a tendon actuated variable curvature section which may be curved in either direction (often with different maximal curvatures in each direction). Section C is a short, straight, rigid segment which houses the tip optics. Section D is a constant curvature concentric tube segment that may be rotated or translated from the base of the scope. This extendible tube has a stiffness that is dominated by the scope. Section E is a straight monopolar cautery wire device with stiffness dominated by the concentric tube.

The robot is manipulated entirely using controls that are proximal to section A. Thus the robot mechanically controls *a)* entry angle, translation and rotation of Section A at the skull, *b)* entry translation and rotation of the internal concentric tube at the tool port, and *c)* entry translation of the cautery wire at the base of the concentric tube.

B. Concentric Tube Design

In designing the components to be extended from the endoscope lumen, attention must be paid to the length and curvature of the concentric tubes to create both an appropriate workspace and a stable robot. To this end, a simulated surgical environment was created using three dimensional MRI images of hydrocephalic ventricles. The model was extracted from a T2 weighted scan using a semi-automated segmentation routine based on differential intensity between the CSF and the surrounding neural tissue. The voxels of the images are accurate to within 1 mm. Following extraction of the volume, a marching cubes smoothing algorithm followed by a Gaussian smoothing operation was applied to obtain the ventricular geometry as shown in Fig. 6. Point targets along the inner surface were chosen by the surgeon to match positions where the choroid plexus is located. Using the 3-dimensional model as a virtual workspace, the ventricular space was integrated with Matlab software that simulates the endoscope, concentric tube, and cautery wire.

It has been shown that cost functions may be used to solve for optimal curvatures within a given workspace [23]. For this robotic design, we consider the manipulation of the manual

endoscope to be a *navigation design problem* coupled with the concentric tube & wire as a *manipulator design problem*. The critical parameters in these algorithms are the curvature and length of the concentric tubes. Due to the interactions that arise when tubes with large curvatures are rotated with respect to each other, those with shorter arc lengths and less curvature will always be more stable [2]. These constraints were balanced against the benefit of an improved workspace that arises from a more tightly curved concentric tube. Ultimately, by solving equations 4–11 from [23] a stable configuration (if available for the workspace) may be found.

Once an appropriate set of tube parameters were determined, the simulator allowed an operator to use the virtual robot in a virtual anatomic space. The user would then navigate the virtual ventricular space and attempt to touch the choroid targets. Using the parameters described in Table I, all target points were successfully hit. Note that as shown in Fig. 6 the most distal point in the ventricular horns can be targeted successfully with the added curved tube, yet it is unreachable without it.

Dimensions of each section of the robotic endoscope are shown in Table I.

C. Actuation Hardware and Electronics

The actuation components can be split into two main subsystems: the ‘tool manipulator’ and the ‘endoscope manipulator’. The tool manipulator controls the actuation of *a)* the concentric tube and, *b)* the cautery wire, both of which pass through the endoscope lumen. As shown in Fig. 7, the components are accessible and well constrained within the region around the lumen entrance. This allows for the use of multiple concentric tube and tool combinations while maintaining the existing endoscope subsystem.

The tool manipulator has three degrees of freedom, with the actuators arranged in a nested configuration. The innermost actuator is a linear control (Firgelli L12505012P) that translates the cautery wire along a miniature linear ball slide with analog position feedback. This wire has uniform stiffness and is straight, and thus positional error does not affect the robot kinematics. The next actuator rotates the concentric tube and cautery wire using a belt-driven brushed DC motor with encoder feedback (Maxon 350579). This entire assembly is mounted on the carriage of a precision ball screw linear actuator (Parker Daedal), driven by a brushed DC motor with encoder feedback (Maxon 339152). The tool manipulator subsystem has been designed to allow convenient substitution of alternate tool assemblies, such as biopsy forceps or a fiber optic laser.

The endoscope manipulator controls five degrees of freedom, each of which would normally be controlled manually by the surgeon. The endoscope body is secured to the center of a frame that can rotate and translate along its central axis. Scope rotation is actuated using a brushed DC motor with encoder feedback that drives a worm gear. This gives precise control and ensures that the scope is not back-drivable despite the weight of the frame. The frame is mounted on a linear ball slide, which is actuated using a linear actuator with analog position feedback (Firgelli FAPO35128). The endoscope neck passes through a gimbaled outer cannula just proximal to the skull insertion point. The two-axis gimbal is actuated using two servo actuators (JRNES517). The variable curvature of the endoscope (section B) is controlled via direct mechanical rotation of the Neuro-Fiberscope lever using a servo actuator (JRNES517). An encoder provides precise angular feedback of the lever.

All of the actuators are controlled by a Simulink model, loaded onto a PC 104 CPU board with two attached Sensoray 526 multifunction I/O boards. The apparatus is controlled using a dual joystick controller with additional control buttons. The PC 104 runs MathWorks’ XPC Target real-time operating environment. The Sensoray boards provide encoder input

and I/O capabilities for the analog sensors and joysticks. An additional microcontroller is used to generate the PWM signals that control the servo-actuators and the cautery wire linear actuator which is controlled by a custom H-bridge circuit. The control loop is run at 1kHz.

D. Robot Control System

The motion control of the robot has been partitioned into two components that mirror the mechanical hardware. Thus there is a control system for the tool manipulator and a control system for the endoscope manipulator. These systems were decoupled to more efficiently contend with the two dissimilar kinematic maps. If the tool manipulator is considered from the viewport frame (i.e. at the tip of the endoscope) there is a straightforward mathematical relationship between the translation and rotation of the concentric tube/cautery wire and the wire tip position. On the other hand there is no similar reliable kinematic mapping for the endoscope due to the flexible neck (section A). Thus the tool manipulator is driven by position commands, while the endoscope manipulator is driven by joint commands. This control organization allows the surgeon to manipulate the endoscope tip (i.e. camera frame) with one set of controls and the tools with a second set of controls. Both control systems are run simultaneously and manipulated using the same handheld controller.

The relevant frames for the robotic endoscope are shown in Fig. 8. For convenience, all frames are designated with the *z*-axis along the central axis of the robot and are shown unrotated along the *z*-axis in the figure. Because the scope neck flexibility is uncontrolled along its length, there is no clearly defined map between the scope world frame (F_0) and the distal frame of the scope neck (F_A). While it is possible to map the region between F_A and the scope tip (F_C) the lack of absolute position at F_A devalues this information. The surgeon controls the relative motion of frame F_C with a joystick and two triggers (rotation, variable curvature, and insertion of the endoscope).

When a surgeon is manipulating the endoscope, they are visualizing the space on a monitor from the perspective of F_C is therefore natural to create a second system to control the tools as they are visualized extending out of the endoscope lumen. The tool manipulator control system actuates the concentric tube insertion and rotation, as well as the cautery wire insertion. The user prescribes velocity commands for the tip of the cautery wire relative to the view frame, and the relevant joint commands are calculated using an algebraic inverse kinematic model. Note the arrangement as shown in Fig. 9.

For a given desired position (x,y,z) and concentric tube radius (r) the joint variables for concentric tube insertion (t), rotation at the endoscope (θ) and cautery wire insertion (w) can be derived as follows. The rotation θ can be trivially calculated as

$$\theta = arctan2(y, x) \quad (1)$$

The distance from the axis d can be calculated as

$$d = \sqrt{x^2 + y^2} \quad (2)$$

The value for ϕ can be derived from the following two equations:

$$d = r(1 - \cos\,\varphi) + w\,\sin\,\varphi \quad (3)$$

$$z = r \sin\varphi + w \cos\varphi \quad (4)$$

Eliminating ***w*** from this equation yields

$$(d - r) \cos\varphi - z \sin\varphi + r = 0 \quad (5)$$

which can be solved as

$$\varphi = arccos\left(\frac{(d-r)}{\sqrt{(d-r)^2 + z^2}}\right) - arccos\left(\frac{(-r)}{\sqrt{(d-r)^2 + z^2}}\right) \quad (6)$$

With this angle, ***w*** can be calculated from (3) and the third joint variable ***t*** can be calculated as

$$t = r\varphi \quad (7)$$

An algebraic model is sufficient beyond F_C because there is minimal curvature interaction between the cautery wire and the concentric tube.

The relative angle transformation for the concentric tube from the motor angle to F_C is calculated using a torsional model as derived in [2] for the regions without interacting curved regions, and a functional approximation for the regions where the scope curvature interacts with the concentric tube curvature.

The control system is programmed into a Simulink real-time XPC platform, and embedded on a PC-104 computer. The inner loop provides PID control of actuator position for the feedback actuation (three degrees are servos which have internal feedback on the device). The outer loop is closed through the surgeon's visual cues from the scope optic system. Velocity commands of the cautery tip frame and endoscope tip frame are processed through a feed-forward control, assigning desired robot dynamic properties and mapping velocities into frame position commands. The dynamic properties are chosen to match the hardware performance. An overview of the control system is shown in Fig. 10.

IV. Experiments

To verify the simulation results and develop a procedural workflow, a mock procedure was performed by the surgeon using a 3D printed ventricular model. The experiment goals were to *a)* confirm the limitations of the endoscope-only system, *b)* verify the simulated range of the concentric tube enhanced endoscope, and *c)* explore the surgical usability.

The experiment was performed in an OR suite at Children’s Hospital Boston. The ventricular model was positioned on a surgical table and a simulated burr hole was created on the left frontal aspect of the mock-up anatomy. The endoscope was navigated into the ventricle using the fiber optic camera and viewing monitors. Twelve target points were marked on the model on both sides of the superior lateral ventricles and down into the temporal horns. The positions of the targets were similar to those shown above in Fig. 6.

In the first trial the surgeon used only the endoscope and cautery wire. He was able to hit 8 of the 12 target points (66%), where the failed targets were located at positions shown as *B* in Fig. 6 deep within the temporal horns. In the second trial, the surgeon used the robotic

endoscope with the concentric tube driven by the hand-held controller. Using this augmented and roboticized system the surgeon was able to hit 100% of the target points. Subjectively, the surgeon reported that after a brief period of control familiarization he was able to navigate the space using the robotic endoscope without difficulty and at a speed that would be comparable to a manual endoscope. Stable and consistent manipulation of the manual endoscope with the concentric tube and cautery wire was not feasible by hand.

V. Conclusion and Future Work

Overall, it is clear that the robotic endoscope offers a number of advantages over a standard manual endoscope when applied to this condition and procedure. It is also clear that a combination of continuum robot design types may have distinct advantages over using a single one when building narrow, flexible robots. Other minimally invasive procedures involving narrow lumens would benefit from the improved workspace as well. For example, this technology would have the potential to improve the sensitivity of targeted transesophageal lung biopsy or colonic/small bowel biopsy. In these constrained environments, this style of device allows for the use of additional degrees of freedom that would otherwise be physically impossible for a surgeon to control. The method of roboticizing an existing technology is may also have advantages when it comes to seeking FDA approval. Future work will focus on the adaptation of the system to additional procedures and anatomical workspaces.

Acknowledgments

We would like to thank Karl Storz Endoscopy America Inc. for use of their endoscopes, Bob Driscoll and Christine Smith for their expertise, and MAXON for their support.

The project described was supported by Grant Number R43EB014063 from the National Institute Of Biomedical Imaging And Bioengineering.

References

1. Maeso S, Reza M, Mayol J, Blasco J, Guerra M, Andradas E, Plana M. Efficacy of the Da Vinci Surgical System in Abdominal Surgery Compared With That of Laparoscopy: A Systematic Review and Meta-Analysis. Annals of Surgery. 2010; vol. 252:254–262. [PubMed: 20622659]
2. Dupont P, Lock J, Itkowitz B, Butler E. Design and Control of Concentric Tube Robots. IEEE Trans Robotics. 2010; 26(2):209–225.
3. Rucker DC, Jones BA, Webster RJ III. A Model for Concentric Tube Continuum Robots Under Applied Wrenches. IEEE Int Conf Robotics and Automation (ICRA). 2010:1047–1052.
4. Lock, J.; Laing, G.; Mahvash, M.; Dupont, P. Quasistatic Modeling of Concentric Tube Robots with External Loads; IEEE/RSJ Int Conf Intelligent Robots and Systems (IROS); 2010. p. 2325-2332.
5. Lock, J.; Dupont, P. Friction Modeling in Concentric Tube Robots; IEEE Int Conf Robotics and Automation (ICRA); 2011. p. 1139-1146.
6. Camarillo D, Milne C, Carlson C, Zinn M, Salisbury JK. Mechanics Modeling of Tendon-Driven Continuum Manipulators. IEEE Trans Robotics. 2008 Dec; 24(6):1262–1273.
7. Robinson, G.; Davies, J. Continuum Robots – A State of the Art; IEEE/RSJ Int Conf Intel Robots & Systems (IROS); 1999. p. 2849-2854.
8. Warf B. Comparison of endoscopic third ventriculostomy alone and combined with choroid plexus cauterization in infants younger than 1 year of age: a prospective study in 550 African children. J Neurosurg (6 Suppl Pediatrics). 2005; 103:475–481.
9. Warf B, Campbell J. Combined endoscopic third ventriculostomy and choroid plexus cauterization (ETV/CPC) as primary treatment of hydrocephalus for infants with myelomeningocele: Long-term results of a prospective intention to treat study in 115 African infants. J Neurosurg Pediatrics. 2008; 2:310–316.

10. Warf B. Endoscopic third ventriculostomy and choroid plexus cauterization for pediatric hydrocephalus. ClinNeurosurg. 2007; 54:78–82.
11. Warf B. Hydrocephalus in Uganda: the predominance of infectious origin and primary management with endoscopic third ventriculostomy. J Neurosurg. 2005; 102:1–15. [PubMed: 16206728]
12. Warf B. Endoscopic coagulation of the choroid plexus in the management of hydrocephalus in developing countries. "Endoscopy and its application to ventricular lesions". 30th Anniversary Supplement to Neurosurgery: "Surgery of the Cerebrum", Part II. 2008; 103:583–584.
13. Cappabianca P, Gangemi M, Rocco FD, Mascari C. Application of neuroendoscopy to intraventricular lesions. Neurosurgery. 2008; vol. 62(no. 2):575–598. [PubMed: 18596446]
14. Apuzzo ML WM, Dobkin WR, Zee CS, Chan JC, Giannotta SL. Surgical considerations in treatment of intraventricular cysticercosis. Journal of Neurosurgery. 1984; vol. 60:400–407. [PubMed: 6607328]
15. Fukushima TT. Endoscopic biopsy of intraventricular tumors with the use of a ventriculofiberscope. . Neurosurgery. 1978; vol. 2(no. 2):110–113. [PubMed: 732959]
16. Gaab MR SH. Neuroendoscopic approach to intraventricular lesions. Journal of Neurosurgery. 1998; vol. 88(no. 3):496–505. [PubMed: 9488304]
17. Macarthur DC RI, Buxton N, Punt J, Vloeberghs M. The role of neuroendoscopy in the management of brain tumours. Br J Neurosurg. 2002; vol. 16(no. 5):465–470. [PubMed: 12498490]
18. Bondurant CP, Jimenez DF. Epidemiology of cerebrospinal fluidshunting. Tediatric Neurosurgery. 1995; 23:254–258.
19. McBeth PB, Louw DF, Rizun PR, Sutherland GR. Robotics in neurosurgery. American journal of surgery. 2004 Oct; vol. 188(no. 4):68S–75S. [PubMed: 15476655]
20. Hongo K, Kobayashi S, Kakizawa Y, Koyama J, Goto T, Okudera H, Kan K, Fujie MG, Iseki H. NeuRobot: Telecontrolled Micromanipulator System for Minimally Invasive Microneurosurgery - Preliminary Results. Neurosurgery. 2002; vol. 51(no. 4):985–988. [PubMed: 12234407]
21. Ho, M.; Desai, J. Towards a MRI-compatible meso-scale SMA-actuated robot using PWM control; ConfProc IEEE EMBS Biomedical Robotics and Biomechatronics (BioRob); 2010. p. 361-366.
22. Madsen JR. Evolution of the Surgical Robot: the Case for Slithering. IEEE ICRA 2010 Full Day Workshop: Snakes, Worms and Catheters: Continuum and Serpentine Robots for Minimally Invasive Surgery.
23. Bedell, C.; Lock, J.; Gosline, A.; Dupont, P. Design Optimization of Concentric Tube Robots Based on Task and Anatomical Constraints; IEEE Int Conf Robotics and Automation (ICRA); 2011. p. 398-403.

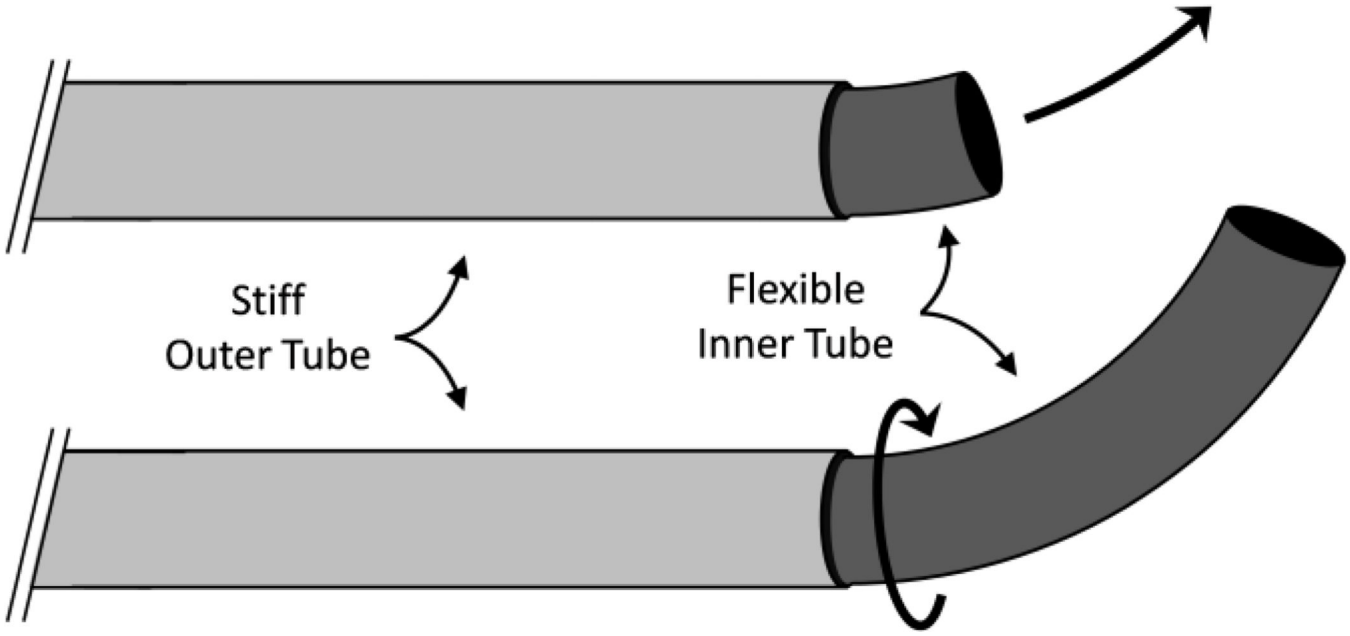

Fig. 1.
One style of mechanism for a concentric tube ‘joint’.

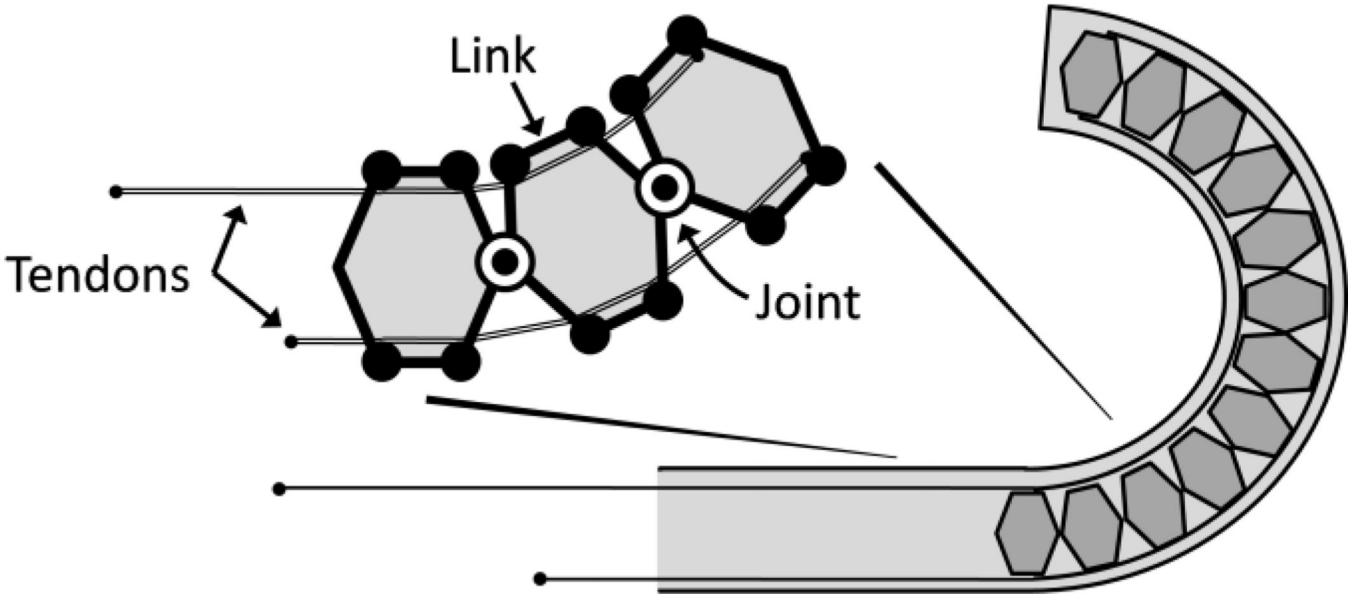

Fig. 2.
Two-dimensional mechanical design for an endoscope tip.

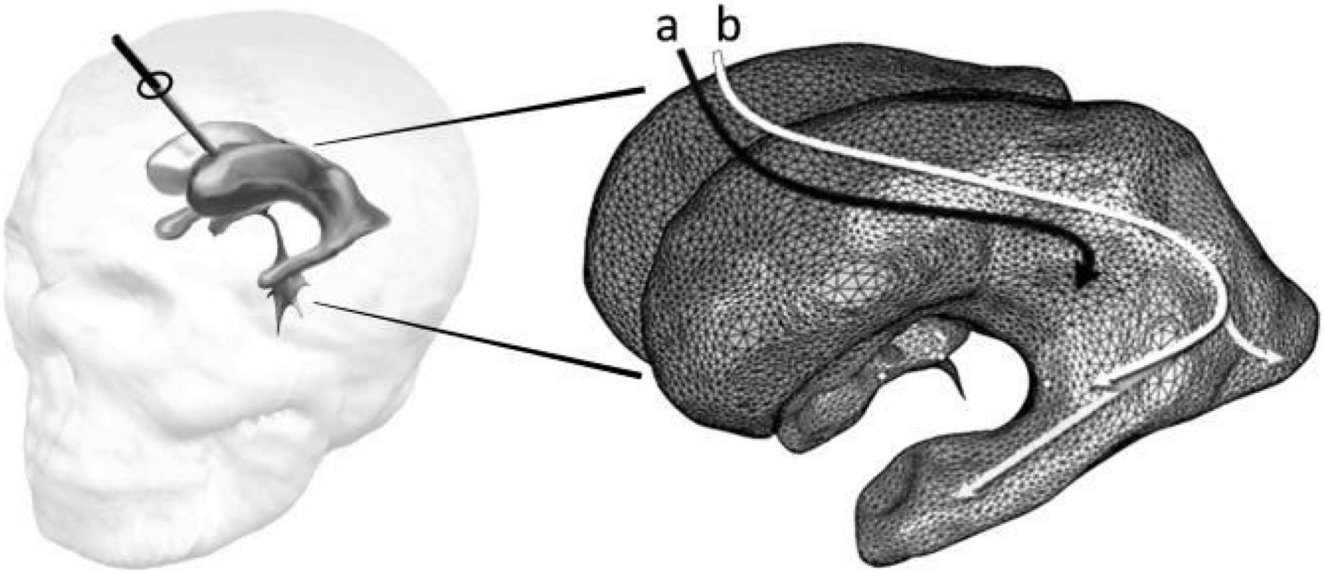

Fig. 3.
Endoscopic entry through the skull and brain into lateral ventricles, showing current access (a) and desired access (b).

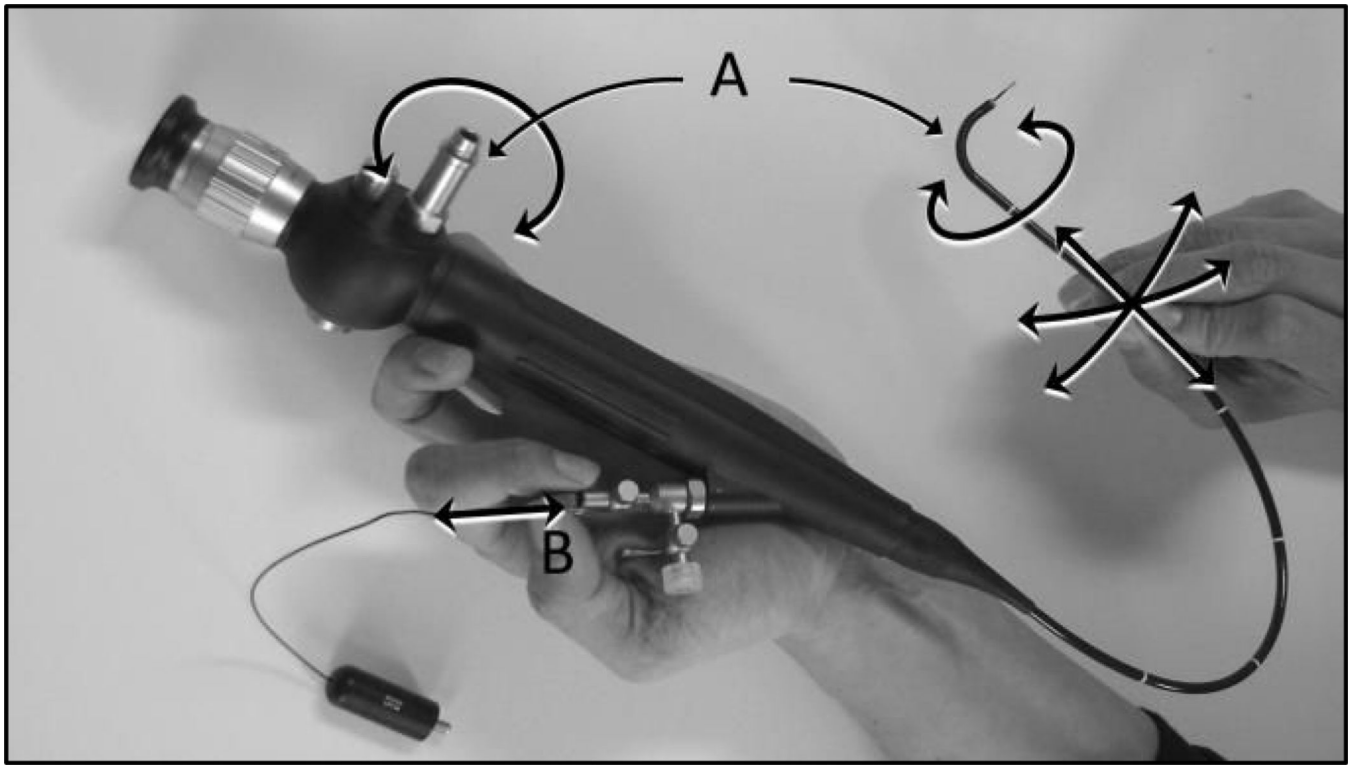

Fig. 4.
Karl Storz Neuro-Fiberscope with tendon-driven tip mechanism (A), flexible neck, and tool port (B).

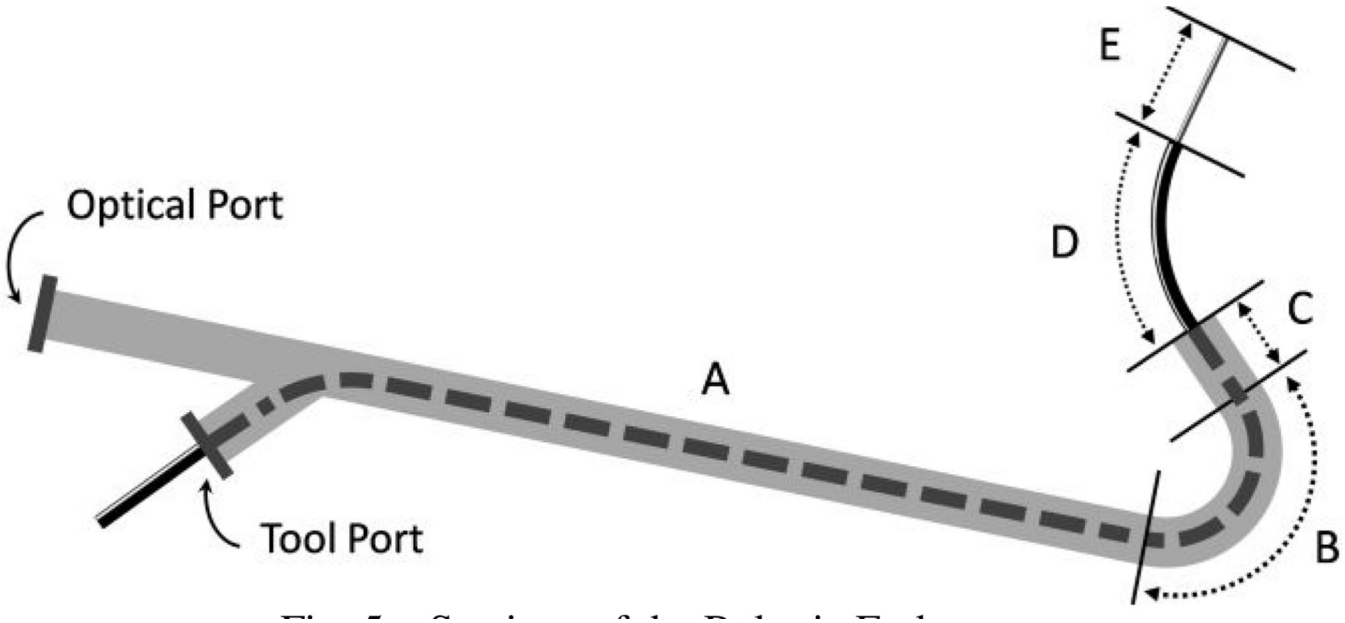

Fig. 5.
Sections of the Robotic Endoscope.

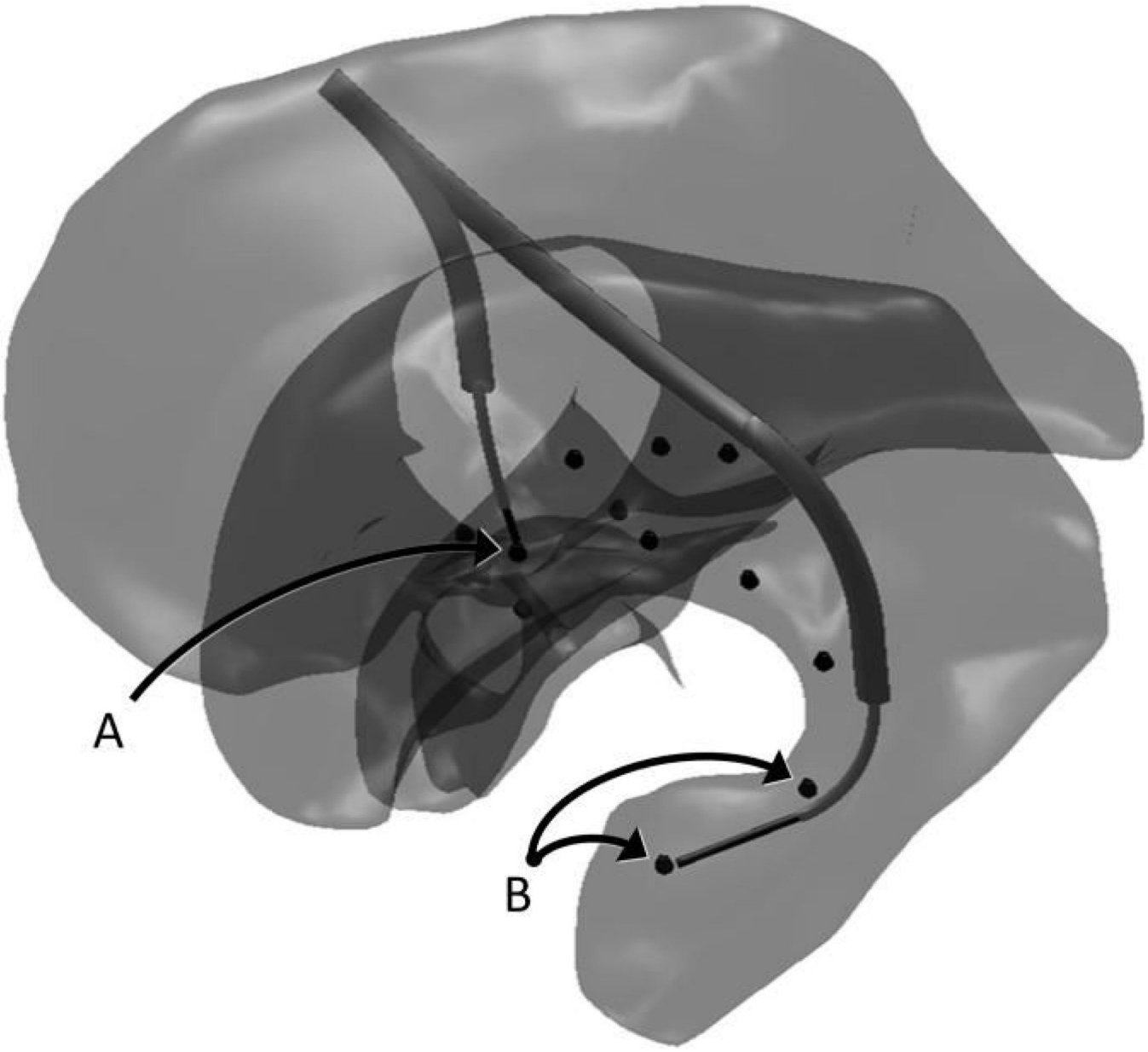

Fig. 6.
In-silica assessment showing cautery wire hitting target in unchallenging position A (superior lateral ventricle) and the more challenging positions B (distal temporal horn).

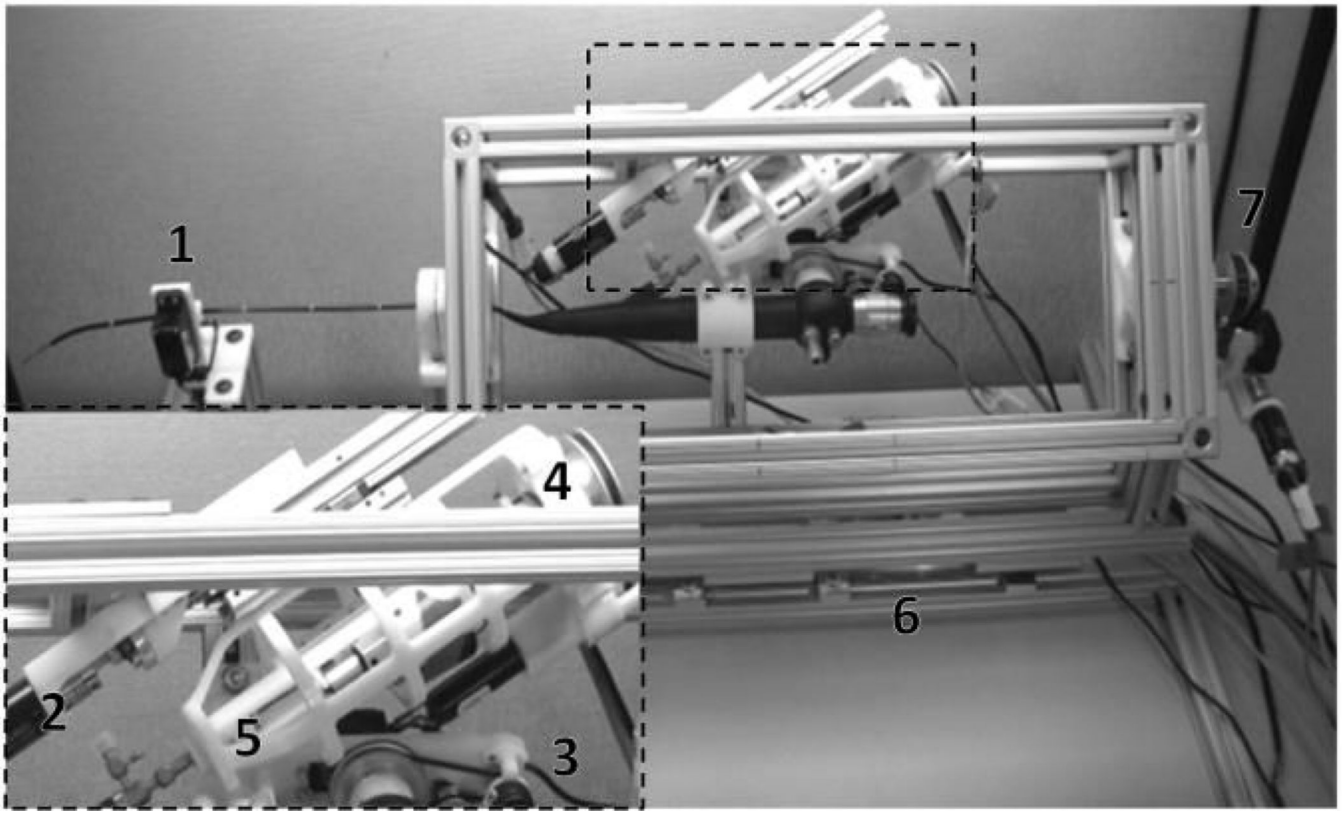

Fig. 7.
Prototype Robotic Endoscope showing (1) Scope neck gimbal, (2) tube insertion, (3) scope tip curvature, (4) tube rotation, (5) wire insertion, (6) scope insertion, and (7) scope rotation.

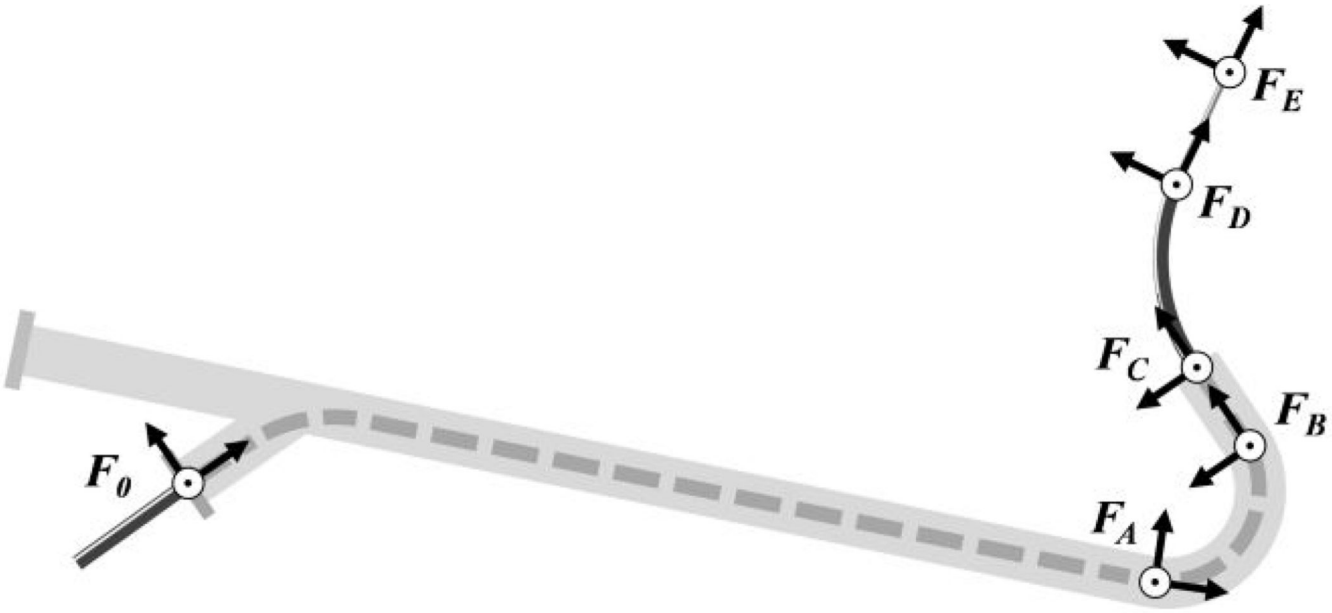

Fig. 8.
Relevant frames for kinematic modeling.

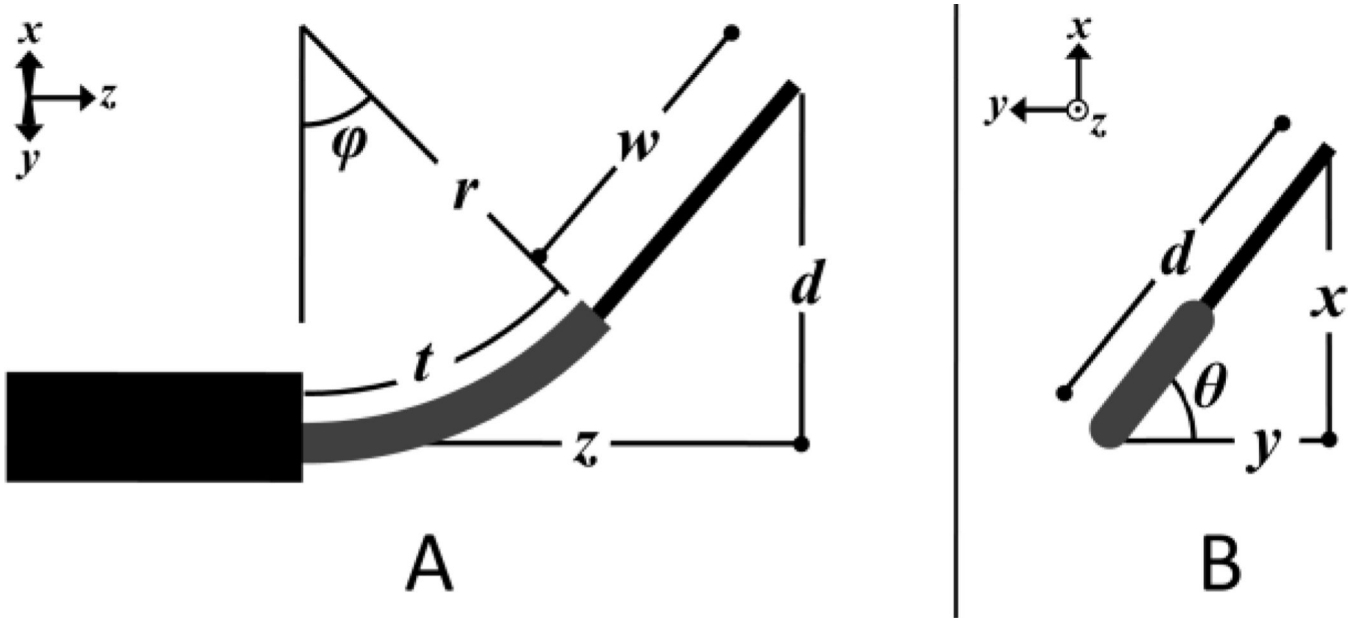

Fig. 9.
Lateral planar view (A) and axial proximal-to-distal view (B) of concentric tube and cautery wire extending from the endoscope tip.

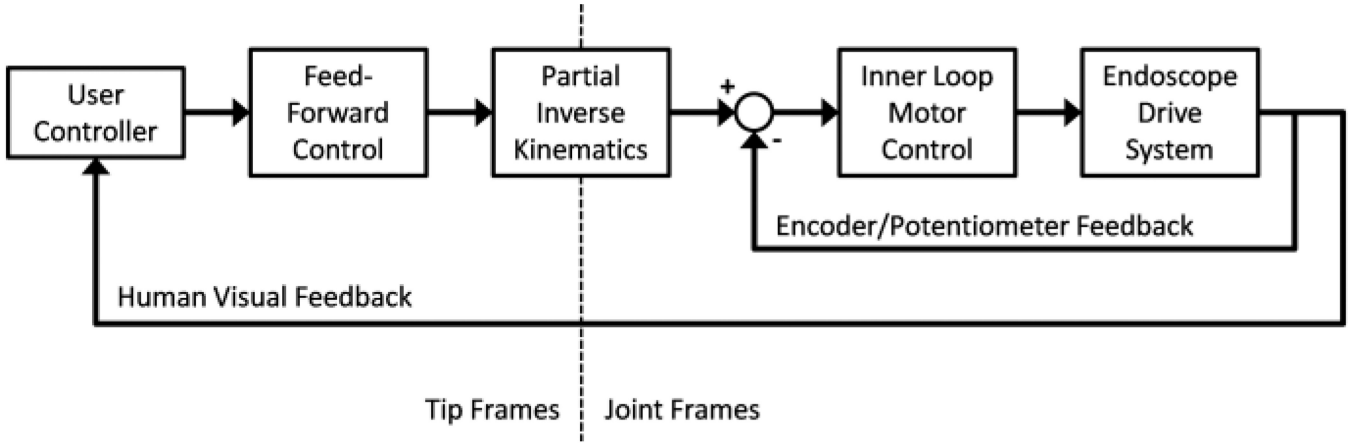

Fig. 10.
Robotic endoscope control system schematic.

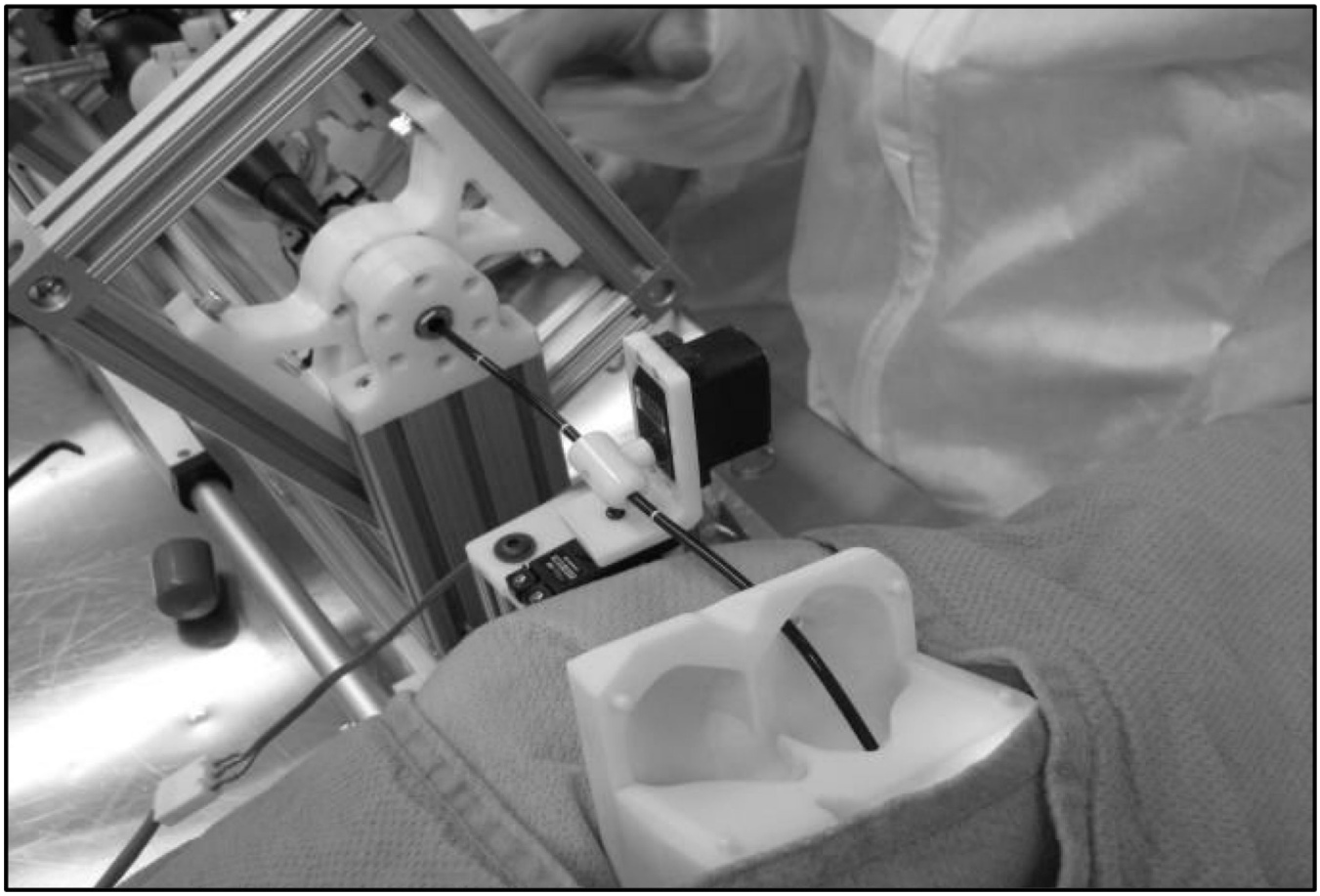

Fig. 11.
Experimental setup, showing robotic endoscope and 3D ventricular model.

TABLE I

Scope and Tube Properties

Endoscope		OD total length	3.7 mm 492 mm
Variable Curvature	*(section B)*	length max angles min radius	25 mm 180,100° 7,12 mm
Tip	*(section C)*	length	8 mm
Concentric Tube	*(section D)*	OD max length	1.3 mm 30 mm
Cautery Wire	*(section E)*	OD max length	1.0 mm 30 mm